

# Molecular dynamics simulations of shear-driven gas flows in nano-channels

Murat Barisik · Ali Beskok

Received: 7 April 2011 / Accepted: 26 May 2011 / Published online: 8 June 2011  
© Springer-Verlag 2011

**Abstract** Using the recently developed smart wall molecular dynamics algorithm, shear-driven gas flows in nano-scale channels are investigated to reveal the surface–gas interaction effects for flows in the transition and free molecular flow regimes. For the specified surface properties and gas–surface pair interactions, density and stress profiles exhibit a universal behavior inside the wall force penetration region at different flow conditions. Shear stress results are utilized to calculate the tangential momentum accommodation coefficient (TMAC) between argon gas and FCC walls. The TMAC value is shown to be independent of the flow properties and Knudsen number in all simulations. Velocity profiles show distinct deviations from the kinetic theory based solutions inside the wall force penetration depth, while they match the linearized Boltzmann equation solution outside these zones. Results indicate emergence of the wall force field penetration depth as an additional length scale for gas flows in nano-channels, breaking the dynamic similarity between rarefied and nano-scale gas flows solely based on the Knudsen and Mach numbers.

**Keywords** Wall force field effects · Tangential momentum accommodation coefficient · Shear stress · Rarefied gas flow

## 1 Introduction

Nano-scale confined gas flows are encountered in the components of micro- and nano-electromechanical systems,

and in magnetic disc drive units (Juang et al. 2007; Tagava et al. 2007). For the latter, distance between the head and media is on the order of 10 nm, and the next generation disc drives strive to reduce this distance to enhance the magnetic storage capacity. Classical approach to study gas flows in such small scales utilizes the kinetic theory. Comparison of the characteristic domain size,  $H$ , with the local gas mean free path,  $\lambda$ , enables definition of the Knudsen number ( $Kn = \lambda/H$ ), which shows the extent of the nonequilibrium and/or rarefaction effects. The flow is categorized to be in the free molecular flow regime for  $Kn \geq 10$ ; in the transition flow regime for  $0.1 \leq Kn \leq 10$ ; and in the slip and continuum flow regimes for  $0.01 \leq Kn \leq 0.1$ , and  $Kn \leq 0.01$ , respectively (Karniadakis et al. 2005). The mean free path for air at standard conditions is about 65 nm. As a result, the aforementioned nano-scale confined flows are mostly in the transition and free molecular flow regimes. Kinetic theory based analyses of these flows utilize analytical and numerical solutions of the Boltzmann equation (Sone et al. 1990; Fukui and Kaneko 1987, 1990), and the direct simulation Monte Carlo method (Bird 1994; Park et al. 2004; Bahukudumbi et al. 2003).

Rarefied gas flows can be characterized by the Reynolds ( $Re$ ), Mach ( $M$ ), and Knudsen ( $Kn$ ) numbers. However, these three parameters for ideal gas flows are interdependent by,

$$Kn = \sqrt{\pi} \frac{\gamma M}{2 Re}, \quad (1)$$

where  $\gamma$  is the ratio of specific heats. As a result, dynamic similarity of rarefied gas flows can be maintained by matching only two dimensionless parameters, preferably the  $Kn$  and  $M$  (Beskok and Karniadakis 1994). Kinetic theory based investigations of nano-scale gas transport assume “dynamic similarity” between the gas flows in low

---

M. Barisik · A. Beskok (✉)  
Institute of Micro and Nanotechnology, Old Dominion  
University, Norfolk, VA 23529-0247, USA  
e-mail: abeskok@odu.edu

pressure environments (i.e., large  $\lambda$ ) and small scale domains. Such characterizations often neglect the surface force interactions between gas and wall molecules. Even for the most simplified case of atomically smooth non-charged surfaces, van der Waals force field interactions between the wall and gas molecules induce variations in momentum and energy transport within the *wall force field penetration depth*, which extends typically three molecular diameters ( $\sim 1$  nm) from each wall. As a result, 40% of a 5.4 nm wide channel would experience the wall force field effects, within which the transport could significantly deviate from the kinetic theory predictions.

Analysis of fluid behavior near a surface requires proper investigations of the wall force field effects. This can be achieved either utilizing simplified wall potential models that ignore the atomic structure of surfaces (Steele 1973), or via three-dimensional molecular dynamics (MD) simulations. Inside the wall force penetration depth, solid surface induces body forces on fluid molecules, which result in surface induced stresses. Stresses generated by the surface–particle interactions are identified as the “surface virial.” Our earlier study was focused on the stress variations in gas, dense gas and liquid argon confined in stationary nanochannels, where the “surface virial” created anisotropic normal stresses for dilute and dense gas phases while the normal stresses became isotropic and recovered the thermodynamic pressure sufficiently away from the surfaces (Barisik and Beskok 2011). These previous studies were performed in stationary channels and employed equilibrium MD simulations. As a result, they did not focus on flow and tangential momentum exchange of gas molecules with walls.

The tangential momentum exchange between a surface and gas can be characterized using the tangential momentum accommodation coefficient, TMAC ( $\alpha$ ), which was introduced by Maxwell as the fraction of gas molecules reflected diffusively from a solid surface. Specifically  $\alpha = 1$  and  $\alpha = 0$  correspond to diffuse and specular reflections, respectively. Despite the presence of other scattering kernels, such as the Cercignani–Lampis model (Cercignani and Lampis 1971), most theoretical and numerical research on rarefied gas flows utilizes Maxwell’s gas–surface interaction model due to its simplicity. As a result, several experimental and numerical studies were conducted for determination of TMAC. Experimental research ranged from molecular beam experiments to gas flow experiments in the slip and early transition flow regimes (Arkilic et al. 2001; Bentz et al. 1997, 2001; Goodman and Wachman 1976; Gronych et al. 2004; Rettner 1998; Sazhin et al. 2001), while the numerical research includes MD simulations of single-molecule interactions with crystalline surfaces (Arya et al. 2003; Chirita et al. 1993, 1997; Finger et al. 2007), two- and three-dimensional MD simulations for  $Kn < 1$  flows (Cao

et al. 2005; Sun and Li 2010, 2011), and coupled MD/DSMC models (Yamamoto et al. 2006).

Fluid behavior in the wall force penetration region depends mostly on the properties of the surface–gas pair. In order to show this, we pick a specific gas–surface pair, and show independency of the near wall fluid behavior on channel dimensions ( $H$ ) and flow dynamics ( $Kn$ ). Therefore, the surface and gas properties, and the surface–gas interaction parameters are kept constant, while the channel height and gas densities are varied to explore and categorize gas flow inside the force penetration depth. MD results are compared with the solutions of the linearized Boltzmann equation in literature (Sone et al. 1990) at various modified Knudsen number ( $k$ ) values, defined as  $k = \left(\frac{\sqrt{\pi}}{2}\right)Kn$ .

The *objective* of this manuscript is to investigate the deviations of nano-scale confined shear-driven gas flows from kinetic theory predictions due to the wall force field effects. This study shows a universal behavior inside the wall force penetration depth, regardless of the characteristic dimensions of confinement, gas density and the Knudsen number. In order to address this, two different sets of molecular dynamics simulations are conducted. In the first set of simulations, we varied  $H$  and density to compare the results of  $k = 10$  flow in different height nanochannels, and studied dimensional effects on dynamically similar flow conditions. In the second set of simulations, we varied the channel height and kept the local pressure and temperature constant, and varied  $k$  from early transition to free molecular flow regime. Thus, we were able to investigate  $k$  dependency of the surface influence. Findings of this research clearly indicate the importance of wall force field effects in nano-scale confinements, mostly neglected in previous gas flow studies.

This paper is organized as follows: in Sect. 2, we describe the MD simulation parameters, explain the stress tensor computations and methods utilized in the MD algorithm. In Sect. 3, we present gas flow results at  $k = 10$  and at various  $k$  values in two sub sections. Comparisons are made on density, normal stress, shear stress, and velocity profiles for each case. Kinetic and virial contributions of shear stresses are investigated separately, and the importance of surface virial terms is presented. MD predictions of shear stress and velocity profiles are compared with the kinetic theory calculations, and TMAC values are predicted. Finally, Sect. 4 presents the conclusions of this study.

## 2 Three-dimensional MD simulation details

We consider argon gas flow confined between two infinite plates that are a distance  $H$  apart as illustrated in Fig. 1.

Periodic boundary conditions were applied in the axial ( $x$ ) and lateral ( $z$ ) directions. Atomistic walls move in opposite directions with a characteristic velocity corresponding to  $U_w = M\sqrt{\gamma k_b T/m}$ , where  $M$  is the Mach number,  $\gamma$  is the adiabatic index (5/3 for monatomic molecules),  $k_b$  is the Boltzmann constant ( $1.3806 \times 10^{-23} \text{ J K}^{-1}$ ),  $T$  is the temperature, and  $m$  is the molecular mass of gas molecules. Mass for an argon molecule is  $m = 6.63 \times 10^{-26} \text{ kg}$ , its molecular diameter is  $\sigma = 0.3405 \text{ nm}$  and the depth of the potential well for argon is  $\varepsilon = 119.8 \times k_b$ . For simplicity, the walls have molecular mass and diameter equivalent to argon ( $m_{\text{wall}} = m_{\text{Ar}}$ ,  $\sigma_{\text{wall}} = \sigma_{\text{Ar}}$ ) with FCC (face-centered cubic) structure, and (1,0,0) plane faces the gas molecules.

Lennard–Jones (L–J) 6–12 potential was utilized to model the van der Waals interactions between gas–gas and gas–wall molecules. In this study, we utilized the potential strength for gas–wall interactions to be the same with that of gas–gas molecular interactions ( $\varepsilon_{\text{wall–Ar}} = \varepsilon_{\text{Ar–Ar}}$ ). Since the L–J potential vanishes at larger molecular distances, only the interactions with particles within a certain cut-off radius ( $r_c$ ) need to be calculated. Therefore, the intermolecular interaction forces were truncated and switched to zero at a certain cut-off distance (Allen and Tildesley 1989). The truncated (6–12) Lennard–Jones (L–J) potential given as:

$$V_{\text{truncated}}(r_{ij}) = 4\varepsilon \left( \left( \left( \frac{\sigma}{r_{ij}} \right)^{12} - \left( \frac{\sigma}{r_{ij}} \right)^6 \right) - \left( \left( \frac{\sigma}{r_c} \right)^{12} - \left( \frac{\sigma}{r_c} \right)^6 \right) \right), \quad (2)$$

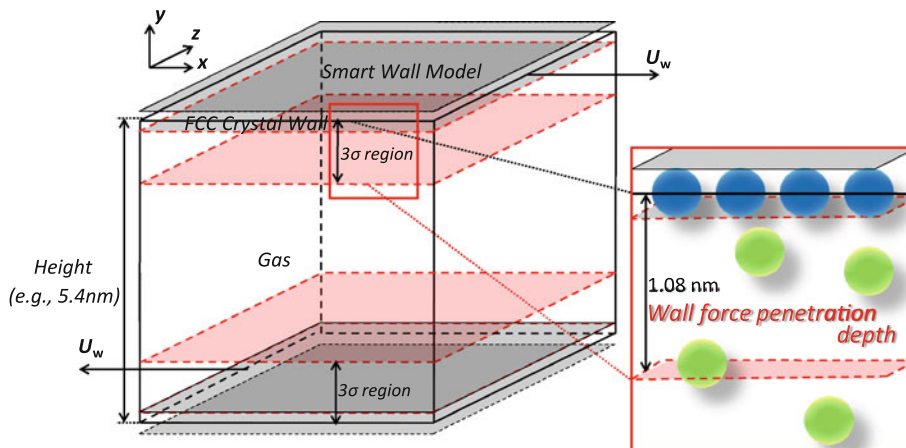
where  $r_{ij}$  is the intermolecular distance,  $\varepsilon$  is the depth of the potential well,  $\sigma$  is the molecular diameter, and  $r_c$  is the cut-off radius. In this study we utilized  $r_c = 1.08 \text{ nm}$ , which is approximately equal to  $3.17\sigma$  for argon molecules. At this cut-off-distance the attractive part of the L–J potential is reduced to  $0.00392\varepsilon$ . Our algorithm utilized the

well known link cell method to handle particle–particle interactions (Allen and Tildesley 1989).

Gas states evolve through intermolecular collisions separated by ballistic motion of particles characterized by the mean free path ( $\lambda$ ). Molecular dynamics (MD) simulations in three-dimensional computational domains need to span at least one mean free path per periodic (lateral and axial) direction in order not to affect the gas intermolecular collisions (Barisik et al. 2010). This requirement renders MD simulations of gas flows computationally overwhelming due to the excessive number of wall molecules. For this reason, MD based studies of nano-scale confined gas flows are quite limited in the literature. In order to address this limitation, we developed a smart wall MD (SWMD) algorithm to reduce the memory requirement of wall modeling (Barisik et al. 2010). For three-dimensional FCC crystal structured wall with  $0.54 \text{ nm}$  cube side length and (1,0,0) plane facing the gas molecules, the SWMD limits memory use of a semi infinite wall slab into a stencil of 74 wall molecules by utilizing the aforementioned cut-off distance for L–J potential, and enables modeling of gas flows within sufficiently large three-dimensional domains. FCC wall structure details are shown in Fig. 2. The current SWMD is a fixed lattice model, where the wall molecules are rigid and keep their corresponding FCC positions (i.e., cold wall model). Hence, there is no thermal motion of wall molecules.

Overall the computational domain sizes were chosen according to  $\lambda$  of the simulated gas states. Thus, for the first simulation set of argon gas flow in the free molecular regime, domain sizes of  $54 \text{ nm} \times 5.4 \text{ nm} \times 54 \text{ nm}$ ,  $108 \text{ nm} \times 10.8 \text{ nm} \times 108 \text{ nm}$ , and  $162 \text{ nm} \times 16.2 \text{ nm} \times 162 \text{ nm}$  ( $\lambda \times H \times \lambda$ ) were selected at different pressures to render  $k = 10$  flow within different channel sizes. For various  $k$  flows at standard conditions, simulations were performed inside  $5.4, 10.8, 27, 54,$  and  $108 \text{ nm}$  height channels with a constant domain span equal to  $54 \text{ nm}$  in length and width. Simulation details can be found in Table 1.

**Fig. 1** Sketch of the simulation domain with explanation of the wall force penetration depth



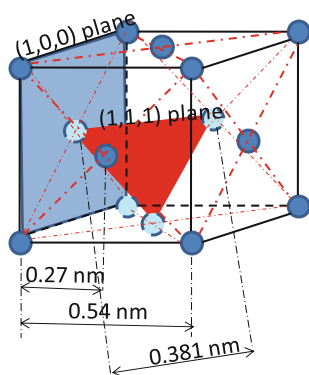


**Fig. 2** The schematics of the unit FCC fixed lattice for solid walls

Simulations started from the Maxwell–Boltzmann velocity distribution for gas molecules at 298 K. Initial particle distribution was evolved  $10^6$  time steps (4 ns) to reach an isothermal steady state using 4 fs ( $\sim 0.002\tau$ ) time steps, after which,  $2 \times 10^6$  time steps (8 ns) were performed for time averaging. Longer time averaging has also been performed to confirm convergence of the density, stress, and velocity profiles to the steady state. Particularly, simulation times were compared with the mean collision times to result in a state amenable for time or ensemble averaging. The mean collision time is predicted by the ratio of  $\lambda$  to the mean thermal speed  $c_m = \sqrt{8RT/\pi}$ , where  $R$  is the specific gas constant ( $208.132 \text{ J K}^{-1} \text{ kg}^{-1}$  for Ar) and  $T$  is the gas temperature. In order to capture the property variations within the near wall region accurately and using the same resolution, all simulation domains were divided into equally sized bins of 0.054 nm in height in the wall normal direction. As a result,  $k = 10$  cases use 100 slab bins, while  $k = 0.5$  case utilizes 2,000 slab bins.

We employed the canonical ensemble (NVT, i.e., constant mole,  $N$ , volume,  $V$ , and temperature,  $T$ ) by utilizing a thermostat. Initially, Nose–Hoover thermostat (Evans and Hoover 1986) was applied to all fluid molecules at each time step to obtain isothermal condition of 298 K with a relaxation time of  $\sim 0.2 \text{ ps}$ . This resulted in temperature variations in the near wall regions even for very low wall

velocities (16 m/s,  $M = 0.05$ ), and became more significant for moderate wall speeds of 64 m/s ( $M = 0.2$ ). Detailed discussions about using Nose–Hoover thermostat for gas simulations are out of scope of this manuscript, and will be presented elsewhere. In order to maintain a constant temperature system in our study, the Nose–Hoover algorithm was employed as a global thermostat inside the local sub-domains. We divided the flow domain into sub-domains having 0.54 nm heights through the entire span which is 10 times larger than the utilized bin size. By this way, similar numbers of particles were obtained inside each sub-domain. Thus, each sub-domain had the same Hamiltonian. Applying the global Nose–Hoover thermostat inside each sub-domain was able to maintain constant temperature in the entire flow domain.

Irving–Kirkwood (I–K) expression was utilized to compute the stress tensor components for an  $N$  particle system with unity differential operator approximation as follows (Irving and Kirkwood 1950, Todd et al. 1995),

$$S_{kl} = \frac{1}{\text{vol}} \left\langle \sum_i^N m^i (V_k^i - \bar{V}_k^i) (V_l^i - \bar{V}_l^i) + W_{kl} \right\rangle, \quad (3)$$

$$W_{kl} = \frac{1}{2} \sum_{i,j}^N (r_k^j - r_k^i) f_l^{i,j}, \quad (4)$$

where the first term on the right hand side of Eq. 3 is the kinetic, and the  $W_{kl}$  term is the virial component. In the kinetic part,  $m^i$  is the atomic mass of particle  $i$ , while  $k$  and  $l$  are the axes of the Cartesian coordinate system,  $V_k^i$  and  $V_l^i$  are the peculiar velocity components of particle  $i$  in the  $k$  and  $l$  directions, and  $\bar{V}_k^i$  and  $\bar{V}_l^i$  are the local average streaming velocities at the position of particle  $i$ , in the  $k$  and  $l$  directions, respectively. The local streaming velocities within each bin were initially calculated and subtracted from the local molecular velocities. For the virial component,  $(r_k^j - r_k^i)$  in Eq. 4 is the  $k$ th component of the relative distance vector between particles  $i$  and  $j$ , and  $f_l^{i,j}$  is the  $l$ th component of the intermolecular force exerted on particle  $i$  by particle  $j$ . Virial of each molecule is calculated according to its interactions with the other molecules that are one cut-of-distance away by using Eq. 4 in the link cell

**Table 1** MD simulation details for argon gas at 298 K

$k = \left(\frac{\sqrt{\pi}}{2}\right) Kn$	Domain $W \times H \times L$ (nm)	# Argon molecules	$\rho$ (#/nm <sup>3</sup> )	$\rho$ (kg/m <sup>3</sup> )	$\rho_{\text{bulk}}$ (#/nm <sup>3</sup> )	$P_{\text{bulk}}$ (kPa)
$k = 10$	$54 \times 5.4 \times 54$	450	0.0286	1.896	0.0275	113.65
	$108 \times 10.8 \times 108$	1800	0.0143	0.948	0.014	58.07
	$162 \times 16.2 \times 162$	4050	0.0095	0.632	0.0094	38.93
$k = 5$	$54 \times 10.8 \times 54$	900	0.0286	1.896	0.028	115.11
$k = 2$	$54 \times 27 \times 54$	1350	0.0286	1.896	0.0283	116.2
$k = 1$	$54 \times 54 \times 54$	4500	0.0286	1.896	0.0285	116.56
$k = 0.5$	$54 \times 108 \times 54$	9000	0.0286	1.896	0.0285	116.73

algorithm. After which, Eq. 3 is applied inside each averaging bin for each time step.

Atomistic stress calculations using the I–K expression require evaluation of the kinetic and virial contributions in Eq. 3. The kinetic component is a function of the particle velocities, and considers momentum of particles. Relating the temperature of a system with its kinetic energy, the equipartition theorem explains ideal gas equivalence of this term, as  $\frac{S_{xx}+S_{yy}+S_{zz}}{3} = \frac{1}{3\text{Vol}} \left\langle \sum_i^N m^i (V_k^i - \bar{V}_k^i)^2 \right\rangle = \frac{NkT}{\text{Vol}} = P$ . Thus, the kinetic part captures the ideal gas law regardless of the fluid's state. The second term in the Irving–Kirkwood expression is the virial part, which considers internal contributions from intermolecular forces between the molecules. Specifically, the virial part shown in Eq. 4 has two additive components originating from particle–particle and surface–particle interactions. For a domain free of solid boundaries, particle–particle virial acts as a correction to the ideal gas law by taking account the particle interactions. Thus, molecular dynamics can estimate the correct thermodynamic state in various density domains by calculating the particle–particle virial terms using a sufficiently large intermolecular interaction cut-off distance. For a detailed investigation of normal stress calculations for gas, dense gas, and liquid domains, the readers are referred to (Barisik and Beskok 2011). Surface force field effects on the stress distribution are calculated using the surface–particle virial, which has significant contributions to all components of the stress tensor within the wall force field penetration region.

### 3 Results

In the following, we present two different sets of results. Initially, we present shear-driven gas flow in the free molecular regime at  $k = 10$  using different size nano-channels at various pressures. This is followed with gas flow at different size channels at fixed pressure and temperature spanning transition and free molecular flow regimes ( $0.5 \leq k \leq 10$ ).

#### 3.1 Gas flows at $k = 10$

We first focus on argon gas flow within 5.4, 10.8, and 16.2 nm height channels at 1.896, 0.948, and 0.632 kg/m<sup>3</sup> densities, respectively (see Table 1). Shear-driven flow is obtained by moving the top and bottom channel walls in opposite directions at the same speed. Density variations at fixed temperature (298 K) result in different pressures and mean free path values. As a result, the channel height is varied to obtain  $k = 10$  flow at different pressures. Kinetic theory based solutions of these flows are identical and

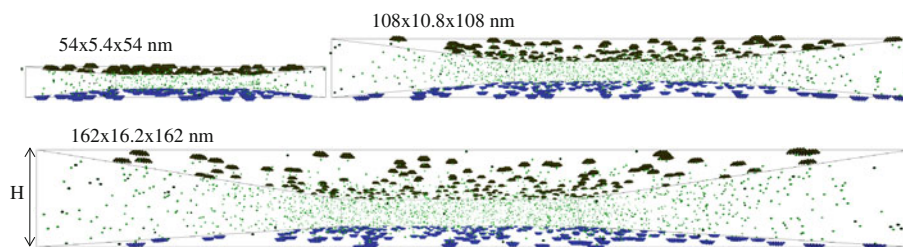
determined by the Knudsen and Mach numbers. Our objective is to test the nano-scale confinement effects by varying the channel height at a fixed  $k$  value. Figure 3 shows snapshots of the simulation domains. Gas molecules are shown in green, while presence of a gas molecule within the wall force penetration region requires utilization of the smart wall stencil on the surface, shown in blue and black on the bottom and top surfaces of the channel, respectively.

Density distributions are plotted in Fig. 4a within 2 nm distance from the top wall of each channel. Density is a constant in the bulk of the channels while near surface regions have density buildup with a single peak point. This density increase is due to the wall force field, which induces increased particle residence time inside the force penetration depth. In particular, density starts to deviate from its bulk value around  $2.5\sigma$  from the wall. For the  $H = 5.4$  nm case, the near wall density buildup decreases bulk density to 96.1% of its assigned value. This density reduction is a result of constant number of gas molecules ( $N$ ) used in MD simulations, which diminishes as the ratio of the wall force penetration depth to channel height decreases. The figure also includes a schematic of the wall and gas molecules, to emphasize the scales involved in the problem. The wall is defined at the center of the first row of wall molecules facing the fluid. As a result, gas molecules cannot penetrate to several bins neighboring the wall, and gas density goes to zero within 0.2 nm from the walls.

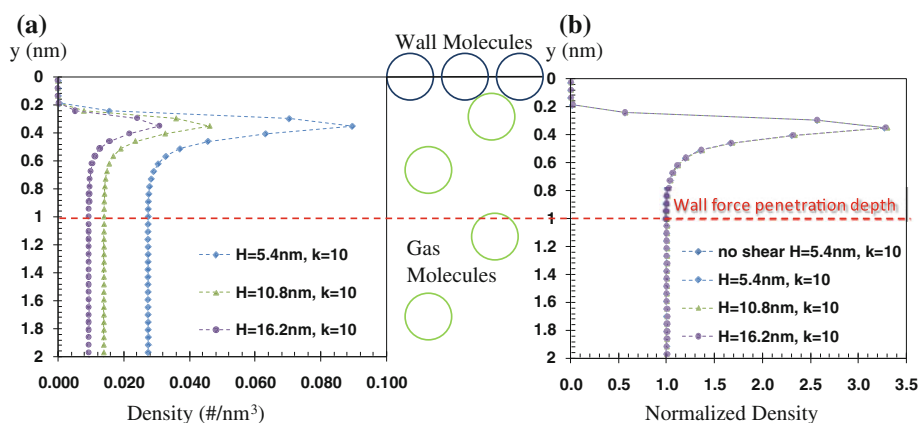
Figure 4b illustrates the density profiles in 5.4, 10.8, and 16.2 nm height channels normalized with the channel center densities of 0.0275, 0.014, and 0.0094 #/nm<sup>3</sup>, respectively. Although the simulations were at different densities, normalized density profiles are identical. Density profile in a 5.4 nm height channel without wall motion (i.e., no-shear) obtained using an NVE system at 298 K is also presented for comparison. Identical density profiles validate our present thermostat technique. The density build-up of each case is linearly proportional to the channel center density. Density variation inside the force penetration depth is a result of the wall force field and only depends on the gas-surface interaction properties. It is unaffected by the channel height, flow, and density.

Figure 5 shows normal stress profiles for  $k = 10$  flows within 2 nm distance from the top wall of each channel. The  $yy$ -components of the normal stress variations are shown in Fig. 5a. Different densities in different height channels led to different stress values. Normal stresses are constant in the bulk regions and equal to pressure based on the ideal gas law, while the walls induce variations inside the force penetration depth. These variations arise from both kinetic and virial contributions of I–K stress calculations due to the density variations and surface-particle interactions, respectively. Since the gas molecules cannot

**Fig. 3** Snapshots of 5.4, 10.8, and 16.2 nm height channel simulation domains at  $k = 10$



**Fig. 4** **a** Density and **b** normalized density distributions for  $k = 10$  flows inside 5.4, 10.8, and 16.2 nm height channels at number densities of 0.0286, 0.0143, and 0.0095  $\#/nm^3$ , respectively. Normalizations are made using the channel center densities of 0.0275, 0.014, and 0.0094  $\#/nm^3$ . The no-shear case corresponds to thermostat free NVE results obtained in 5.4 nm height channel at  $k = 10$  and 298 K



penetrate to the bins neighboring the wall, stress values reach zero very near the walls ( $\sim 0.2$  nm). Figure 5b, c shows the  $yy$ - and  $xx$ -components of the normal stresses, normalized using the channel center values of 113.65, 58.07, and 38.93 kPa for the 5.4, 10.8, and 16.2 nm height channels, respectively. Exact match is obtained between the normal stresses in different density domains indicating independency of the wall force field penetration depth behavior to the characteristic dimensions of the domain, gas density, and flow. The normal stress profiles obtained in a stationary (i.e., no-shear) NVE system are also shown in Fig. 5a, b, and c. The  $yy$ - and  $xx$ -components of normal stresses in the no-shear system are identical with the stress profiles obtained for shear-driven gas flow. This shows that the normal stresses in shear-driven nano-flows are unaffected by the tangential wall motion, as expected. In addition, identical results obtained between the NVE system and the current results validate our present thermostat technique. An important result in Fig. 5 is that the normal stresses are anisotropic in the wall force field penetration region. In fact,  $xx$ - and  $zz$ -components of normal stresses are identical, while the  $yy$ -component of normal stress differs due to differences in the surface virial effects. Detailed investigation of normal stress distributions inside stationary nano-scale channels can be found in (Barisik and Beskok 2011).

Gas velocity profiles normalized with the wall velocity (64 m/s) are plotted in Fig. 6a. The velocity components in  $y$ - and  $z$ -directions have zero average values, confirming one dimensional flow in  $x$ -direction (not shown for

brevity). We show the velocity profiles within half of the nano-channel. In order to compare the bulk portions of the velocity profile with each other, we present velocity variation as a function of the non-dimensional channel height ( $y/H$ ). The velocity profiles obtained using linearized Boltzmann equation at  $k = 10$  subjected to the TMAC ( $\alpha$ ) values of  $\alpha = 1$  and  $\alpha = 0.75$  are also presented. The MD based velocity profiles agree well with the kinetic theory predictions adopted from reference (Sone et al. 1990) in the middle of the channels. Better match between the MD results and linearized Boltzmann solutions using TMAC value of  $\alpha = 0.75$  is observed for all cases. MD results show sudden changes in the velocity profile within the force penetration depth (i.e., approximately 1 nm away from each surface). Overlays of this region on flow domains are differently visualized in Fig. 6a due to the use of different channel heights and utilization of normalized distance ( $y/H$ ) in the figure. In order to clarify the influence of the wall force field, we zoom on the velocity profiles within 2 nm from the top wall in Fig. 6b. Identical velocity variations in the near wall region are observed despite of different shear rates in the bulk region, and different channel heights. Gas velocity increases rapidly within the force penetration region, and suddenly goes to zero on the walls, since the gas molecules cannot penetrate to several bins immediately neighboring the wall. Extrapolation of the velocity profile on to the walls shows reduction in the velocity slip for this particular case, which could be as a result of  $\epsilon_{\text{wall-Ar}}/\epsilon_{\text{Ar-Ar}} = 1$  used in this study. This is a drastic difference from the linearized Boltzmann equation

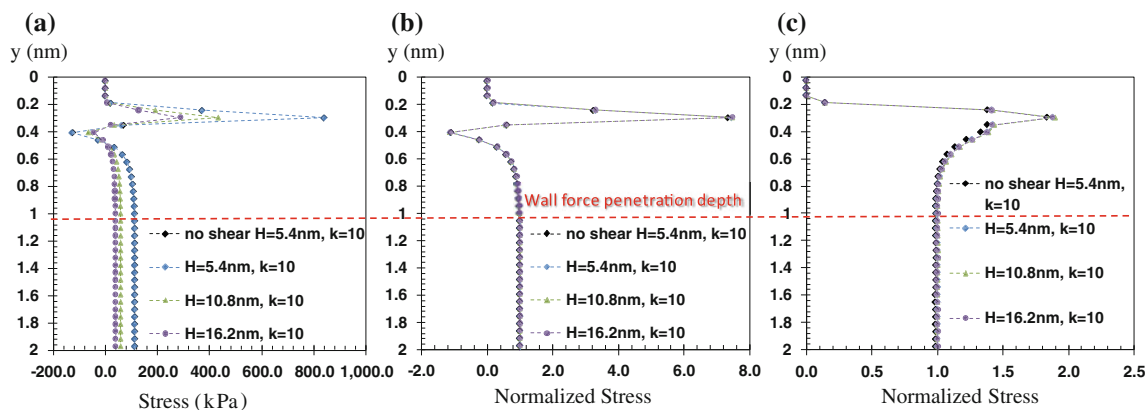


**Fig. 5** **a** Dimensional, and **b** normalized  $yy$ -components, and **c** normalized  $xx$ -components of normal stress distributions of  $k = 10$  flows inside 5.4, 10.8, and 16.2 nm height channels at 0.0274, 0.014, and 0.0094 #/nm<sup>3</sup>, respectively. Normalizations are made using the

channel center values of 113.65, 58.07, and 38.93 kPa. The no-shear case correspond to thermostat free NVE results of 5.4 nm height channel at  $k = 10$

solutions at different TMAC values, which indicate substantial velocity slip on the walls.

Shear stress distributions in the nano-channels are plotted in Fig. 7 within 2 nm distance from the top wall of each case. In Fig. 7a constant wall velocity of 64 m/s ( $M = 0.2$ ) results in various shear rates inside different height channels. Since the channel velocity was kept constant, the shear stresses vary linearly with the shear rate; proving linear stress–strain rate relationship for constant  $k$  flows. This and the earlier results on density and normal stress variations show that simulations are in the linear shear response region (i.e., applied shear rate does not induce any non-linear effects). Shear stress values are constant in the bulk region, while the surface virial induces variations near the walls with single peak points that are linearly proportional to the bulk shear stress values. In order to compare the shear stress profiles at a constant shear rate, wall velocities are adjusted according to the channel heights. Figure 7b shows shear stress variation in channels moving at  $M = 0.1, 0.2,$  and  $0.3$  for the 5.4, 10.8 and 16.2 nm height channels, respectively. Shear stress

variations within the wall force penetration region in different sized channels at a constant shear rate are identical. This validates linear shear response and linear stress–strain rate relationship for constant  $k$  flows inside the nano-confinements.

Shear stresses are constant in the bulk of the channels, and show variations within 0.34 nm ( $\sim \sigma$ ) from wall. In order to explain the surface force effects on shear stress, we present in Fig. 8, the shear stress variation within 5.4 nm channel as the sum of its kinetic and virial contributions. Shear stress is defined by the kinetic term in most of the domain. Using a similar definition, kinetic theory based solution techniques utilize the kinetic evolution of molecules to calculate shear stresses only by considering particle velocities. The figure shows that the kinetic component of shear stress goes to zero within approximately  $\sigma$  distance from the wall. However, the surface virial increases starting from one sigma distance from wall till the impenetrable zone for gas molecules where the density diminishes (i.e.,  $0.2 \text{ nm} \leq y \leq 0.34 \text{ nm}$ ). Interestingly, density and density related properties are in a

**Fig. 6** Normalized velocity profiles of  $k = 10$  flows with constant wall velocity of 64 m/s **a** as a function of normalized channel height ( $y/H$ ), and **b** within 2 nm distance from the walls

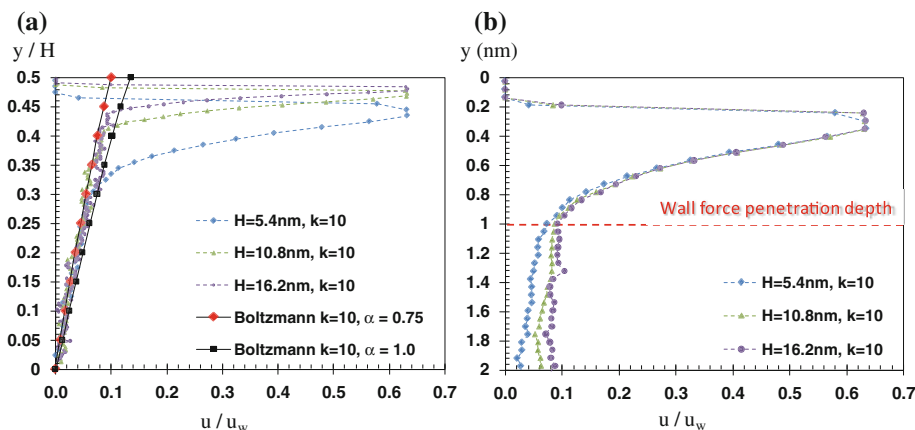
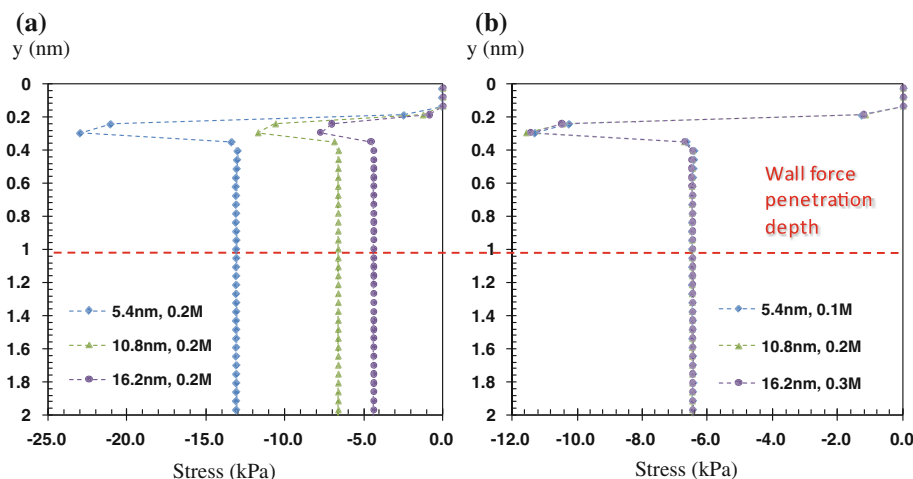


**Fig. 7** Shear stress distributions in 5.4, 10.8, and 16.2 nm height channels at  $k = 10$  with **a** constant wall velocity of 64 m/s ( $M = 0.2$ ), and **b** constant shear rate at  $M = 0.1, 0.2,$  and  $0.3$ , respectively



decreasing trend in the same region while the surface virial term peaks. This region, from one sigma distance to zero density, is the main location where the wall and gas molecules interact with strong repulsive forces.

Based on the kinetic theory of gases, shear stress for shear-driven flow in the free molecular flow regime ( $Kn \rightarrow \infty$ ) can be written as (Fukui et al. 2005),

$$\tau_\infty = -\frac{\alpha}{2-\alpha} \rho U \sqrt{\frac{RT_w}{2\pi}} \tag{5}$$

where  $T_w$  is the wall temperature (298K). The TMAC value can be interpreted as  $\alpha$  portion of molecules reflecting diffusively, while and  $(1 - \alpha)$  portion reflecting specularly. As can be seen, pure specularly reflecting wall will not drive the fluid, and result in zero shear stress, while lower TMAC values will result in lower shear stress. We cannot directly apply Eq. 5 to predict the TMAC value for our simulations at  $k = 10$ . In order to consider the finite

Knudsen number effects we utilized the following correction uniformly valid in the free molecular to slip flow regimes (Bahukudumbi et al. 2003).

$$\frac{\tau}{\tau_\infty} = \frac{0.5297Kn^2 + 1.206Kn}{0.5297Kn^2 + 1.6277Kn + 0.603} \tag{6}$$

Utilizing Eqs. 5 and 6, we predicted the TMAC value for argon gas flow confined in different height channels at  $k = 10$  to be  $\alpha = 0.75$ . Theoretical shear stress values calculated for TMAC values of 1.0 and 0.75, and MD results are shown in Fig. 9a for 5.4 nm height channel. This result shows that the atomically smooth FCC wall structures using  $\epsilon_{wall-Ar}/\epsilon_{Ar-Ar} = 1$  does not exhibit full diffusive reflection. Our studies with other  $\epsilon$  ratios (not shown for brevity) have consistently shown that the TMAC value and shear stress decreases with decreased the  $\epsilon_{wall-Ar}$  value. We verified the consistency of our shear stress results with the velocity profile. Figure 9b shows the kinetic theory prediction of velocity distribution for  $k = 10$  flow at TMAC values of  $\alpha = 1$  and  $\alpha = 0.75$ . We observed that the linearized Boltzmann solution for  $\alpha = 0.75$  matches the MD based velocity predictions better than the  $\alpha = 1$  case in the bulk flow region. Same approach is conducted on all cases of different channel heights with constant wall velocity or constant shear rate conditions. A constant TMAC value ( $\alpha = 0.75$ ) is found for all cases, independent of the channel height, density, channel velocity, and applied shear rate.

### 3.2 Gas flows at various $k$

Shear-driven gas flows in nano-channels are investigated in the early transition to free molecular flow regime by simulating argon gas at 298 K and 116 kPa inside 5.4, 10.8, 27, 54, and 108 nm height channels. Simply by changing the channel heights and keeping the domain density constant, we obtained the  $k = 10, 5, 2, 1,$  and  $0.5$  flows. Thus,

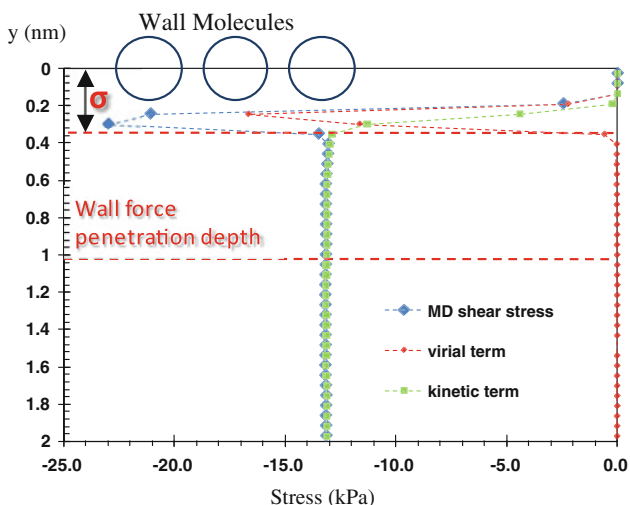


**Fig. 8** Virial and kinetic components of shear stress distribution in 5.4 nm height nano-channel at  $k = 10$



we were able to investigate  $k$  dependency of the surface influence from early transition to free molecular flow regimes. Since all simulations are at the same density,  $\lambda$  is constant. Thus, computational domain spans  $\lambda$  in periodic directions for all cases. Figure 10 shows the simulation domains for different height channels, corresponding to different  $k$  values.

Figure 11a shows density distributions within 2 nm distance from the top wall of each domain. Density is a constant in the bulk region, and increases in the near wall region due to the increased residence time of molecules under the surface effects. For the 5.4 nm height channel, bulk density reduces to 96.1% of its assigned average value due to increased density near the walls. This density reduction in the bulk region vanishes as the channel height increases and becomes negligible for the 108 nm case. Density profiles are identical both in the bulk and in the force penetration regions despite different channel heights and  $k$  values.

The  $yy$ - and  $xx$ -components of normal stresses are shown in Fig. 11b, c, respectively. The normal stress profiles are identical for all cases. Three mutually orthogonal components of the normal stresses are constant and equal in the bulk region. Hence, the pressure is calculated using averaged normal stress, and was found to be  $\sim 116$  kPa for each case, which is equal to the ideal gas predictions. Inside the force penetration depth, normal stress profiles are non-isotropic. This behavior emerges from the surface virial term due to the wall effects.

Velocity profile for  $k = 1$  flow ( $H = 54$  nm) in half of the channel and the linearized Boltzmann solution at  $k = 1$  using  $\alpha = 1.0$  and  $0.75$  are plotted in Fig. 12a. Despite thermal fluctuations due to the use of very small bins, MD results agree better with the theory using  $\alpha = 0.75$  in the bulk region, while deviations from the kinetic theory solution are still observed inside the force penetration depth. Since these deviations are confined in the  $3\sigma$  region, their influence extends only 4% of the domain for 54 nm

height channel. Figure 12b shows velocity profiles for various  $k$  flows within 2 nm distance from the top wall. Different profiles inside the force penetration depth shows effects of the Knudsen number on the near wall velocity profiles. Velocities in the near wall region increase with decreased  $k$  values due the rarefaction effects.

Constant wall velocity used in all cases (64 m/s) creates different shear rates depending on the channel height and  $k$  value. Figure 13a shows shear stress distributions in various  $k$  flows. Shear stress is constant up to one sigma distance from the wall. After which, surface virial component induces variations near the walls with single peak points linearly proportional to the bulk shear stress values. Constant shear cannot be achieved by simply adjusting the wall velocities, since the resulting shear response for different Knudsen flows is different. In order to make a comparison of shear stress variations inside the force penetration depth, we normalized the shear stress values with their corresponding bulk values of  $-13.17$ ,  $-12.91$ ,  $-11.21$ ,  $-9.42$ , and  $-7.73$  kPa for the 5.4, 10.8, 27, 54, and 108 nm height channels, respectively. Figure 13b shows identical normalized shear stress distributions in the force penetration region for all five cases. Hence, the normalized shear stress variation in the near wall region is independent of the channel dimensions, shear rate and the Knudsen number.

Theoretical shear stress values are calculated using Eq. 5 with finite Knudsen number correction in Eq. 6 for various  $k$  values. Similar with the earlier cases, we predicted the TMAC values for argon gas flow at  $k = 0.5, 1, 2, 5,$  and  $10$  to be  $\alpha = 0.75$ .

### 4 Conclusions

The SWMD results of shear-driven argon gas flows in nano-channels revealed significant wall force field effects on the velocity, density, shear stress, and normal stress

**Fig. 9** **a** MD shear stress profile of 5.4 nm height channel at  $k = 10$  flow with wall velocity of 64 m/s and the corresponding theoretical shear stress results for TMAC values of  $\alpha = 1.0$  and  $0.75$ . **b** A zoomed version of the  $k = 10$  flow velocity distributions of MD results and linearized Boltzmann solutions at  $\alpha = 1.0$  and  $0.75$

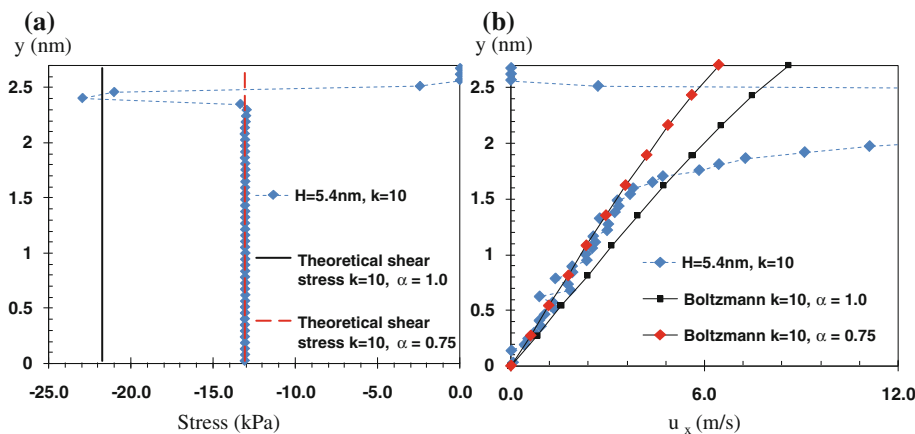


**Fig. 10** Snapshots of simulation domains for argon gas flow inside 5.4, 10.8, 27, 54, and 108 nm height channels, corresponding to  $k = 10, 5, 2, 1,$  and  $0.5$  flows at 298 K and 116 kPa, respectively

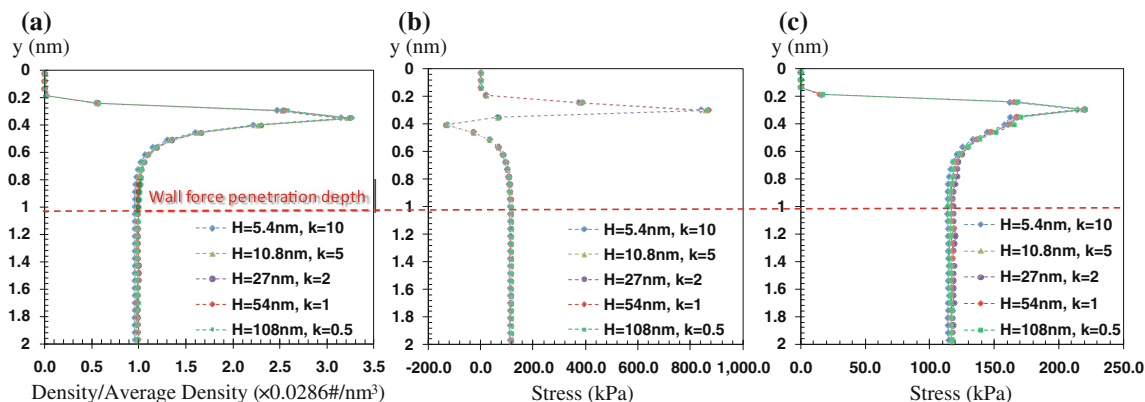
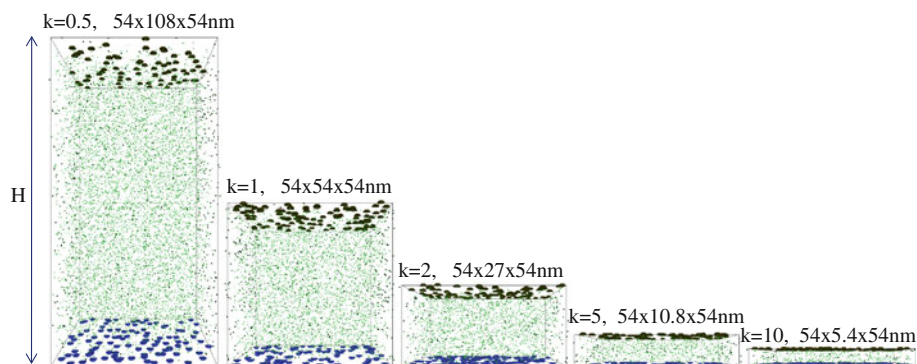
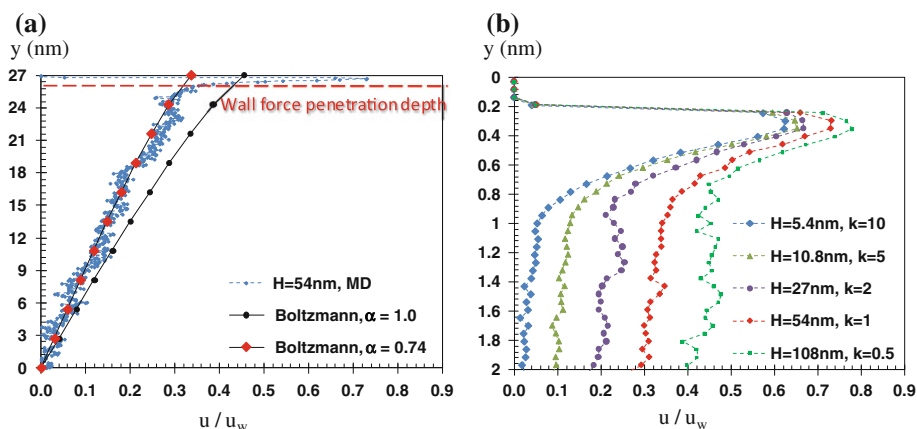


**Fig. 11** **a** Density distribution, and the  $yy$ -components (**b**) and  $xx$ -components (**c**) of normal stresses within 2 nm distance from wall for different  $k$  values

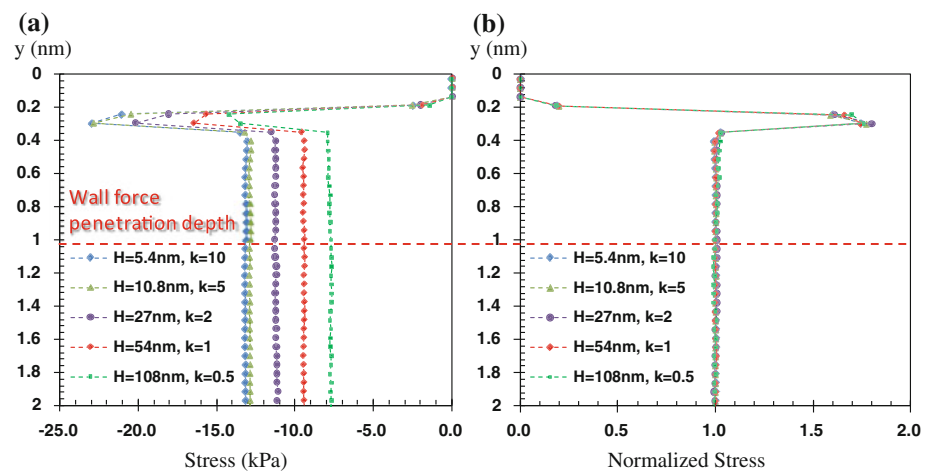
**Fig. 12** **a** Velocity profile for  $k = 1$  flow in half of the 54 nm height channel with linearized Boltzmann solutions using  $\alpha = 1.0$  and  $0.75$ . The domain is divided into 1000 bins. **b** Velocity profiles for various  $k$  flows within 2 nm distance from the top wall. The wall velocity is 64 m/s



distributions in the near wall region that extends about  $3\sigma$  from each surface. Within this region a density build-up with a single peak point is observed. Normal components of the stress tensor are anisotropic, and dominated by the surface virial. Results show that the density and normal stress variations are scalable by the bulk density and pressure, and their behavior are unaffected by the shear-driven flow, channel dimensions, and gas rarefaction. The velocity profiles show sudden increase in gas velocity within this region. This behavior is independent of the

channel dimensions and density, however, varies as a function of the Knudsen number due the rarefaction effects. Outside the “near wall” region, pressure is defined by the ideal gas law and the velocity distribution is predicted by kinetic theory based on the Boltzmann equation. Shear stress values are constant in the bulk region, while the surface virial induces variations very near the walls with a single peak point scalable with the bulk value. Simulation results verify linear stress strain-rate relationship at constant Knudsen values. Another important aspect of our

**Fig. 13** **a** Shear stress distribution for  $k = 10, 5, 2, 1,$  and  $0.5$  flows confined in  $5.4, 10.8, 27, 54,$  and  $108$  nm height channels at constant wall velocity of  $64$  m/s ( $M = 0.2$ ). **b** Shear stress variation within  $2$  nm from the wall, normalized with  $-13.17, -12.91, -11.21, -9.42,$  and  $-7.73$  kPa for the  $5.4, 10.8, 27, 54,$  and  $108$  nm height channels, respectively



findings is that one can predict the TMAC using 3D SWMD simulations. As a result, atomically smooth FCC crystal walls with (1,0,0) plane facing the gas resulted in  $TMAC = 0.75$ , independent of the Knudsen number in the transition and free molecular flow regimes.

Over all the results show that the wall force field penetration depth is an additional length scale for gas flows in nano-channels, breaking the dynamic similarity between rarefied and nano-scale gas flows solely based on the Knudsen and Mach numbers. Hence, one should define a new dimensionless parameter as the ratio of the force field penetration depth to the characteristic channel dimension, where the wall effects cannot be neglected for large values of this dimensionless parameter.

**Acknowledgment** This work was supported by the National Science Foundation under Grant No. DMS 0807983.

## References

- Allen MP, Tildesley DJ (1989) Computer simulation of liquids. Oxford Science Publications, Oxford University Press, New York
- Arkilic EB, Breuer KS, Schmidt MA (2001) Mass flow and tangential momentum accommodation in silicon micromachined channels. *J Fluid Mech* 437:29–43
- Arya G, Chang HC, Maginn EJ (2003) Molecular simulations of Knudsen wall-slip: effect of wall morphology. *Mol Simul* 29(10–11):697–709
- Bahukudumbi P, Park JH, Beskok A (2003) A unified engineering model for steady and quasi-steady shear-driven gas microflows. *Microscale Thermophy Eng* 7:291–315
- Barisik M, Beskok A (2011) Equilibrium molecular dynamics studies on nanoscale confined fluids. *Microfluid Nanofluid*. doi:10.1007/s10404-011-0794-5
- Barisik M, Kim B, Beskok A (2010) Smart wall model for molecular dynamics simulations of nanoscale gas flows. *Commun Comput Phys*. doi:10.4208/cicp.2009.09.118
- Bentz JA, Tompson RV, Loyalka SK (1997) The spinning rotor gauge: measurements of viscosity, velocity slip coefficients, and tangential momentum accommodation coefficients for N<sub>2</sub> and CH<sub>4</sub>. *Vacuum* 48(10):817–824
- Bentz JA, Tompson RV, Loyalka SK (2001) Measurements of viscosity, velocity slip coefficients, and tangential momentum accommodation coefficients using a modified spinning rotor gauge. *J Vac Sci Technol A* 19(1):317–324
- Beskok A, Karniadakis GE (1994) Simulation of heat and momentum transfer in complex micro-geometries. *J Thermophys Heat Transf* 8(4):647–655
- Bird GA (1994) Molecular gas dynamics and the direct simulation of gas flows. Oxford Science Publications, Midsomer Norton, Avon, UK
- Cao BY, Chen M, Guo ZY (2005) Temperature dependence of the tangential momentum accommodation coefficient for gases. *Appl Phys Lett*. doi:10.1063/1.1871363
- Cercignani C, Lampis M (1971) Kinetic models for gas-surface interactions. *Transp Theory Stat Phys* 1:101–114
- Chirita V, Pailthorpe BA, Collins RE (1993) Molecular dynamics study of low-energy Ar scattering by the Ni(001) surface. *J Phys D Appl Phys* 26(1):133–142
- Chirita V, Pailthorpe BA, Collins RE (1997) Non-equilibrium energy and momentum accommodation coefficients of Ar atoms scattered from Ni(001) in the thermal regime: a molecular dynamics study. *Nucl Instrum Methods Phys Res B* 129(4):465–473
- Evans DJ, Hoover WG (1986) Flows far from equilibrium via molecular-dynamics. *Annu Rev Fluid Mech* 18:243–264
- Finger GW, Kapat JS, Bhattacharya A (2007) Molecular dynamics simulation of adsorbent layer effect on tangential momentum accommodation coefficient. *J Fluids Eng*. doi:10.1115/1.2375128
- Fukui S, Kaneko R (1987) Analysis of ultra-thin gas film lubrication based on the linearized Boltzmann equation: influence of accommodation coefficient. *JSME Int J* 30:1660–1666
- Fukui S, Kaneko R (1990) A database for interpolation of Poiseuille flow rates for high Knudsen number lubrication problems. *J Tribol* 112:78–83
- Fukui S, Shimada H, Yamane K, Matsuoka H (2005) Flying characteristics in the free molecular region (influence of accommodation coefficients). *Microsyst Technol*. doi:10.1007/s00542-005-0538-0
- Goodman FO, Wachman HY (1976) Dynamics of gas-surface scattering. Academic Press, New York

- Gronych T, Ulman R, Peksa L, Repa P (2004) Measurements of the relative momentum accommodation coefficient for different gases with a viscosity vacuum gauge. *Vacuum* 73(2):275–279
- Irving JH, Kirkwood JG (1950) The statistical mechanical theory of transport processes. IV. The equations of hydrodynamics. *J Chem Phys* 18:817–829
- Juang JY, Bogy DB, Bhatia CS (2007) Design and dynamics of flying height control slider with piezoelectric nanoactuator in hard disk drives. *ASME J Tribol* 129:161–170
- Karniadakis GE, Beskok A, Aluru N (2005) *Micro flows and nano flows: fundamentals and simulation*. Springer-Verlag, New York
- Park JH, Bahukudumbi P, Beskok A (2004) Rarefaction effects on shear driven oscillatory gas flows: a DSMC study in the entire Knudsen regime. *Phys Fluids* 16(2):317–330
- Rettner CT (1998) Thermal and tangential-momentum accommodation coefficients for N<sub>2</sub> colliding with surfaces of relevance to disk-drive air bearings derived from molecular beam scattering. *IEEE Trans Magn* 34(4):2387–2395
- Sazhin OV, Borisov SF, Sharipov F (2001) Accommodation coefficient of tangential momentum on atomically clean and contaminated surfaces. *J Vac Sci Technol A* 19(5):2499–2503
- Sone Y, Takata S, Ohwada T (1990) Numerical analysis of the plane Couette flow of a rarefied gas on the basis of the linearized Boltzmann equation for hard sphere molecules. *Eur J Mech B/Fluids* 9:273–288
- Steele WA (1973) The physical interaction of gases with crystalline solids I. Gas–solid energies and properties of isolated adsorbed atoms. *Surf Sci* 36:317–352
- Sun J, Li ZX (2010) Two-dimensional molecular dynamic simulations on accommodation coefficients in nanochannels with various wall configurations. *Comput Fluids*. doi:[10.1016/j.compfluid.2010.04.004](https://doi.org/10.1016/j.compfluid.2010.04.004)
- Sun J, Li ZX (2011) Three-dimensional molecular dynamic study on accommodation coefficients in rough nanochannels. doi:[10.1080/01457632.2010.509759](https://doi.org/10.1080/01457632.2010.509759)
- Tagava N, Yoshioka N, Mori A (2007) Effects of ultra-thin liquid lubricant films on contact slider dynamics in hard-disk drives. *Tribol Int* 40:770–779
- Todd BD, Evans DJ, Davis PJ (1995) Pressure tensor for inhomogeneous fluids. *Phys Rev E*. doi:[10.1103/PhysRevE.52.1627](https://doi.org/10.1103/PhysRevE.52.1627)
- Yamamoto K, Takeuchi H, Hyakutake T (2006) Characteristics of reflected gas molecules at a solid surface. *Phys Fluids*. doi:[10.1063/1.2191871](https://doi.org/10.1063/1.2191871)